Research Article | Vol. 27, No. 5 | 4 Mar 2019 | OPTICS EXPRESS 7513
Optics EXPRESS

Compact compound-eye imaging module based on the phase diffractive microlens array for biometric fingerprint capturing

TIANCHI YANG,[1] YAN-HUA LIU,[1,3] QUANQUAN MU,[2] MING ZHU,[1] DONGLIN PU,[1] LINSEN CHEN,[1] AND WENBIN HUANG[1,4]

[1]*School of Optoelectronic Science and Engineering & Collaborative Innovation Center of Suzhou Nano Science and Technology, Soochow University, Suzhou 215006, China*
[2]*State Key Lab of Applied Optics, Changchun Institute of Applied Optics, Fine Mechanics and Physics, Chinese Academy of Sciences, Changchun, Jilin 130033, China*
[3]*yhliu@suda.edu.cn*
[4]*wbhuang@suda.edu.cn*

Abstract: A compound-eye imaging system based on the phase diffractive microlens array as a compact observation module is proposed. As compared with the refractive microlens in common compound-eye imaging systems, the diffractive microlens is a flat imaging optics featuring high relative aperture, thin component thickness and compatibility with lithography techniques. As an application, a compact fingerprint imaging module was demonstrated using this compound-eye imaging system. The phase Fresnel microlens array with continuous trough morphology was fabricated via the self-developed gray-scale laser direct write equipment. An image reconstruction method is proposed by extracting the effective image information of each Fresnel microlens, removing the complex signal separator layer from the compound-eye imaging system. The illumination optics is further planarized through the waveguide backlighting and the waveguide functions as the touch panel for fingerprint recording. The novel compound-eye imaging device length was only restricted by the focal length of the microlens with a low limit of 4.12 f . The applicability of this novel compound-eye imaging system was further demonstrated by recording the human fingerprint texture, paving ways for various applications as a compact imaging system.

1. Introduction

Nature has developed a number of unique architectures with attractive and useful optical functions and scientists have been able to mimic some of those natural structures and realize excellent functions for various applications [1–3]. Among them, biologically inspired compound-eyes, with advantages of fast movement detection, wide field of view and polarization sensing, are being highly pursued and hold great potential for various integrated optical microsystems [4–6]. In artificial compound eye systems, the basic imaging unit, which is called ommateum in a natural compound eye, is commonly represented by a compact artificial imaging system, which consists of a microlens for imaging and a photodetector for sensing [7,8]. The basic artificial unit in a specific direction captures part of the scene and yields a unit image containing part effective information. The superposition of all unit images creates an omnidirectional imaging system for medical imaging, fingerprint capturing and surveillance cameras [9–11]. However, the functionalities of the artificial compound-eye imaging device performance are still inferior to those of the biological counterpart and enormous effects are being made to increase the image depth, the field of view and the imaging quality.

To pursue high-performance optics of artificial compound-eyes, a high fidelity microlens array is highly desirable. Refractive lenslets have been widely utilized in the realization of

#357810 https://doi.org/10.1364/OE.27.007513
Journal © 2019 Received 15 Jan 2019; revised 8 Feb 2019; accepted 12 Feb 2019; published 27 Feb 2019

Optics EXPRESS

artificial compound-eyes due to the similarity to the biological compound-eye and the availability of the maturing fabrication techniques. However, when it comes to optics miniaturization, refractive optics suffer from lens surface curvature, small numerical apertures and increased difficulty in fabrication. On the other hand, flat imaging optics such as the diffractive lens or the metalens are attracting increasing interest for both fundamental and application activities [12–14]. The flat optics rely on micro/nano-meter surface features to obtain a delicate phase control over the whole wavefront for various light modulation purposes. Inherently, these flat optics have advantages of high relative aperture, thin component thickness and large volume fabrication capability [15,16]. As a typical planar optics, the Fresnel lens has been demonstrated in applications such as holograms [17], light harvesting [18], laser processing [19] and waveband-selective diffraction [20]. The performance improvement of the artificial compound-eye system using the Fresnel lens is of significance in terms of both scientific and industry interests, however, to the best of knowledge, it has not been reported yet.

Biometrics techniques using the information of a living body have become a prominent alternative to conventional password schemes that can improve user convenience and network security [21,22]. The biometric recognition device identifies the user through an authentication of physiological, physical, or behavioral characteristics. Optical fingerprint identification approaches are attracting much attention due to the reliability in fingerprint identification and the imperviousness to both environmental electromagnetic interference and electrostatic discharge [23]. To date, optical fingerprint sensors with bulky sizes have been demonstrated and commercialized using the frustrated total internal reflection at a right-angle prism or a direct collection of the finger scattered backward light by single or multiple cameras [24–26]. As a compact imaging module, the artificial compound-eye imaging system holds great promise for the realization of the compact optical fingerprint capturing device.

In literature, there are two types of Fresnel lenses, one is based on the amplitude modulation which consists of alternating opaque and bright zones, and the other is based on the phase modulation in which the phase in each ring zone undergoes a gradient change. The phase Fresnel lens with a higher efficiency is advantageous to the amplitude one, considering that half region in the latter case is opaque. However, one has to divide the one ring zone into multiple regions to obtain a delicate control over the phase, exhibiting high difficulty and complexity for fabrication techniques [27,28]. As a result, most studies on diffractive optics in terms of imaging application purposes are with the amplitude Fresnel lenses [29]. In this work, we propose and demonstrate a compact compound-eye imaging module using the phase Fresnel microlens array for biometric fingerprint capturing purposes. Arraying phase Fresnel microlenses with continuous trough morphology were fabricated to improve the imaging efficiency. The diffractive microlenses had a high relative aperture of 1 and were transferred onto flexible substrates through nanoimprinting for the demonstration of volume production. An image reconstruction method is proposed by extracting the effective information of each unit-image, removing the complex signal separator layer. A LED light source with narrow bandwidth was employed for illumination and is further planarized through the waveguide backlighting. The applicability of this novel compound-eye imaging system was demonstrated by recording the human fingerprint texture and clear fingerprint images were obtained.

2. Device design and architecture

The architecture of the proposed compound-eye imaging module for fingerprint capturing is shown schematically in Fig. 1(a). It is composed of a top glass plate, a diffractive microlens array and an image sensor, providing compact and lightweight hardware through planarization of the imaging lenses. The top glass plate in the system, regarded as the cover glass of the smart phone, functions not only as the touch panel for fingerprint collection, but also as the waveguide for guiding light emitted from the glass edge in order to illuminate the

Optics EXPRESS

fingerprint. The diffractive microlens array, with a design flexibility in the focal distance, the diameter and the working wavelength, is a planar optics for high resolution imaging at a short distance. In addition, we have removed the separator layer, which is frequently implemented in previous compound-eye imaging systems to prevent signal cross-talk [6], in order to simply and compactify the whole imaging system. As for each unit diffractive microlens, it could be regarded as an elemental imaging system, giving a unit image following the imaging law. The proposed system is set to focus on the surface of the top glass plate, yielding a set of unit images called a compound image. We have set a very short object distance in this compact imaging system, and each unit microlens observes a part of the fingerprint determined by the microlens location and the viewing angle. As a result, the unit-images have different sampling information, and they can be utilized for the reconstruction of the final complete fingerprint image. Due to absence of the separator layer, lights from some positions of the fingerprint would be imaged in different unit-images when transmitting through adjacent microlenses, giving rise to signal cross-talk. Therefore, we have tried to directly omit the redundant information in each unit image to stitch together the whole fingerprint image during post-processing, removing the adverse effects of the signal cross-talk. In order to not lose the fingerprint information, the magnification ratio of the microlens imaging system is set as less than unity. The imaging principle of the system is shown in Fig. 1(b). The illuminating light from the edge light source is coupled into the top glass plate via the slanted edge and lights bearing the total internal reflection angles would propagate along the top glass, lighting up the whole glass plate. When a finger touches the top surface, propagating lights would be scattered or remain reflected in the glass at the fingerprint ridge or the groove, producing contrast when imaged from the below microlens array.

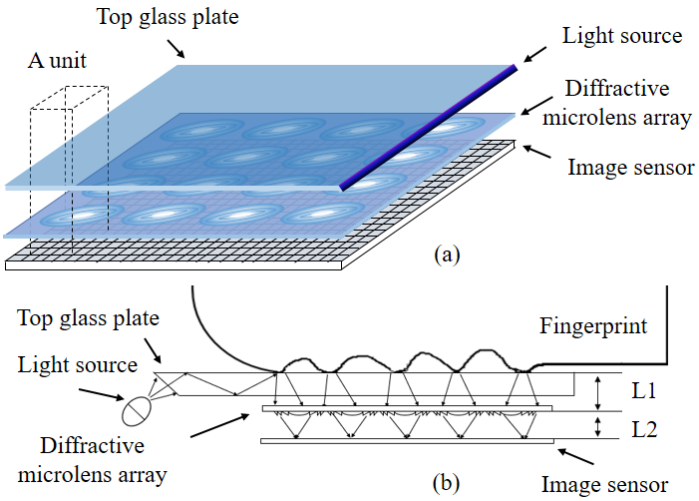

Fig. 1. (a) Schematic diagram of the fingerprint capturing system which is consisted of the top glass plate, the edge illuminating light source, the diffractive microlens array sheet and the image sensor. (b) Side view showing the imaging principle of the system. Illuminating lights in the waveguide are scattered at the fingerprint ridges, existing as bright regions in the image plane.

3. Experimental details

In this work, we fabricated arraying phase Fresnel microlenses by wafer-level microfabrication and proposed its application in the compact fingerprint capturing system. Moreover, the high efficiency Fresnel microlenses with continuous trough morphology could be produced in volume scale by the nanoimprint technique. To this end, we have developed a laser direct write system which is capable of high-resolution (0.5 μm) grayscale lithography with a wafer-scale sample area (6 inch). The main fabrication steps of the diffractive

Optics EXPRESS

microlens array are schematically depicted in Fig. 2, firstly we calculated parameters of the diffractive microlens depending on the desired focal length, aperture, and working wavelength, and then we loaded the grayscale diffractive microlens image into the laser direct write system. After that, the maskless lithography system wrote the grayscale microlenses pattern into the positive photoresist with a thickness 3 μm on the glass substrate (Fig. 2(a)), followed by the immersion of the sample in the developer. As the developing speed of the photoresist depends on the exposure dosage, the relief morphology of the diffractive microlens could be controlled by the exposure intensity and the developing conditions (Fig. 2(b)), thereby resulting in a precise phase control in each ring region. The relief morphology of the diffractive microlens in the photoresist was then transferred onto the nickel plate by electro-plating (Fig. 2(c)), providing a complementary patterned mold with high fidelity and durability. Finally, the nickel mold was brought in contact with a glass substrate or a PET substrate with the UV curable resin filling between them. This was followed by UV light exposure through the transparent substrate and the mold was released from the supporting substrate (Fig. 2(d)), resulting in a diffractive microlens array with continuous trough morphology (Fig. 2(e)).

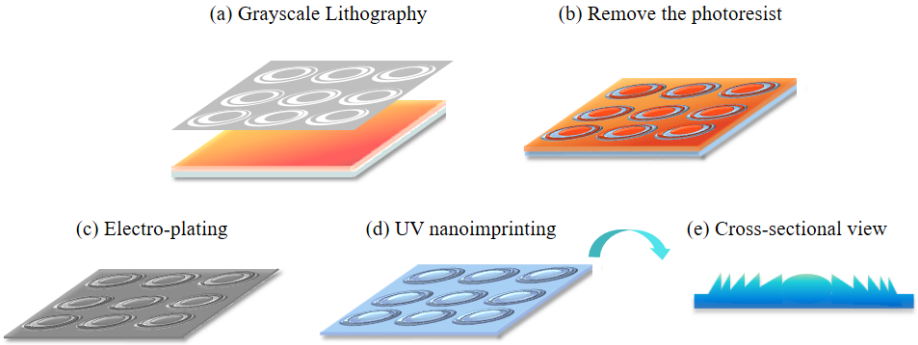

Fig. 2. Schematic illustration of the micro-fabrication process of the diffractive microlens array. (a) High resolution grayscale lithography. (b) Development of the sample to obtain the diffractive microlens array in the photoresist with a continuous relief morphology. (c) Transfer of the pattern onto the nickel mold by electro-plating. (d) Fabrication of the diffractive microlens array with the UV nanoimprinting technique. (e) Schematic illustration of the cross-section of the diffractive microlens showing a continuous morphology.

To obtain a balance between the microlens fabrication difficulty and the imaging performance of the compound-eye system, parameters of the unit diffractive microlens were designed with the aperture and the focal length both being 1 mm. The diffractive microlens was also designed to work under the wavelength of 532 nm considering the utilized LED light source. The illuminating light was coupled into a glass substrate through a slant edge with an efficiency around 50%. We utilized a complementary metal oxide semiconductor array (CMOS, Daheng optics, MER-500-7 UM/UC) as the image sensor (Resolution 2592 × 1944, pixel pitch 2.2 μm). Restricted by the image sensor area we have designed a diffractive microlens array with 5 × 4 units and the microlens pitch is 1 mm to obtain a closely packed microlens array. The grayscale laser direct write system completed writing the whole pattern into the photoresist in half an hour. We obtained the final microlens sheet according to the process in Fig. 2. The entire system was assembled and the object distance and the image distance were adjusted using mechanical actuators by hand with an accuracy of 10 μm. A human finger touched the top glass plate as the object for real-time capturing.

4. The phase diffractive microlens array

The focusing performance of both the amplitude modulated diffractive microlens and the phase modulated one would be unified by the theoretical equation of the multi-level

Optics EXPRESS

diffractive lens $\eta = \left[\sin\left(\frac{\pi}{N}\right)\Big/\frac{\pi}{N}\right]^2$, where η is the focusing efficiency of the diffractive lens and N is the number of steps in a phase period of π [24]. When the step number is 2, the theoretical efficiency is 40.5% which is the case of the amplitude diffractive microlens. As the step number N increases, the focusing efficiency increases monotonously to approach 100%. Morphological investigations by scanning electron microscopy (SEM) and atomic force microscopy (AFM) into the fabricated diffractive microlens in this study are shown in Fig. 3. According to the Fresnel lens equation, the fabricated diffractive microlens has an innermost radius r_1 of 23 μm with 230 zones. Figures 3(a)-3(c) provide scanning electron microscope (SEM) images of the fabricated diffractive microlens from the top view, the cross-sectional view and the tilted view, respectively. As expected, the diffractive microlens consists of decreasing concentric ring bands extending outward from the center. From the top view, the ring bands appear homogeneous with decent morphology. The innermost ring radium was measured to be 23.3 μm which agrees well with the theoretical calculation. The cross-sectional and the titled views imply a continuous trough morphology for the innermost ring and outer rings, enabling a continuous phase change in each ring band with an expected high light efficiency. The AFM images of the diffractive microlens in Figs. 3(d) and 3(e) show more details of the ring trough morphology, in which the height of the measured region is 1.35 μm, yielding a slope angle of 29.3°. We further investigated the slope angle of the ring tough from the innermost ring to the outermost ring and found it should increase from 7.43° to 70° as the ring band goes outward to obtain an optimum focusing efficiency, however, due to the photochromic and mechanical properties of the photoresist, the trough slope angle was limited to 45° at the outermost ring, decreasing the optical efficiency to around 80%. We further investigate the focusing characteristics of the fabricated diffractive microlens array to verify its imaging properties. The microlens array image in Fig. 4(a) was obtained by putting the microlens array in close contact with the CCD camera. It shows a 5 × 4 microlens array with a microlens pitch of 1 mm and a microlens diameter of 1 mm. The CCD imaging plane was then moved to the focusing plane of the diffractive microlens array. The image in Fig. 4(b) shows an array of focusing spots arising from corresponding microlenses. The focal length could be measured by the moved distance of the CCD camera from Figs. 4(a) and 4(b), which was determined to be 0.967 mm. The intensity distribution of the focusing spot is given in Fig. 4(c). Light was intensely concentrated in the spot with a size of 5 μm, determined by the diffraction limit. As a result, the diffractive microlens array is suitable for high resolution imaging at short distances.

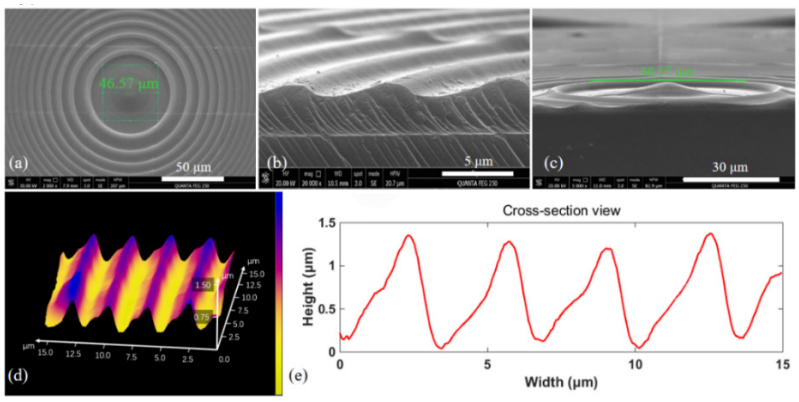

Fig. 3. Morphological images of the diffractive microlens by grayscale lithography. (a) Top view, (b) cross sectional view and (c) tilted view at the angle of 45° of the diffractive microlens by SEM. (d), (e) The morphological profile of the diffractive microlens in different ring bands by AFM.

Optics EXPRESS

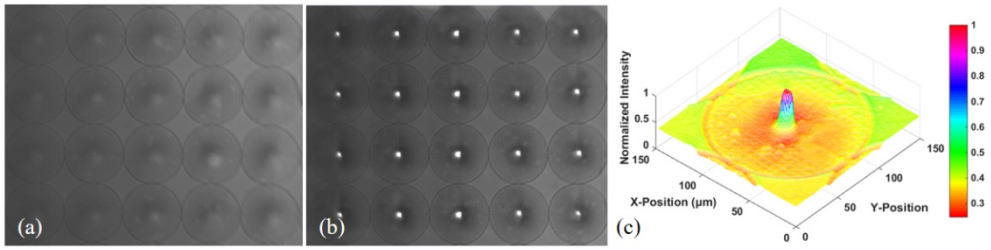

Fig. 4. Focusing properties of the diffractive microlens array. (a) Image of the diffractive microlens array captured by the CCD camera when they are in close contact. (b) Image of the light spots captured by the CCD camera on the focus plane. (c) Focusing spot profile on the CMOS camera showing the light intensity distribution.

5. Principles of information extraction

We start from the investigation into the imaging of the unit diffractive microlens with a focal length of f. According to the paraxial imaging law.

$$\frac{1}{L_1}+\frac{1}{L_2}=\frac{1}{f}$$

Where L_1 and L_2 are the object distance (the distance from the upper surface of the top glass to the diffractive lens array sheet) and the image distance (the distance from the diffractive lens array sheet to the image sensor), respectively, giving rise to a magnification ratio of $m=L_2/L_1$. In addition, the field of view angle ω could be calculated from $\tan\left(\frac{\omega}{2}\right)=\frac{2L_2}{D}$ as shown in Fig. 5(a), where D is the diameter of the unit microlens. The magnification ratio m is equal or less than unity in order to retrieve all information of the fingerprint from the compound image formed by all unit images. We next classify the microlenses into two categories depending on the location and the corresponding influence on the imaging post processing, *i. e.*, the microlenses surrounded by other microlenses (denoted as the middle microlens) and the microlenses on the boundaries (denoted as the boundary microlens). As an illustration, the middle microlens in Fig. 5(a) images part of the fingerprint with a size of D/m into the corresponding sub-image with a size of D. Some part of the fingerprint (II, II*, III and III*) would be captured by different microlenses and forms repeated images on the image sensor, giving rise to undesired signal crosstalk in the original compound image. Thus, we have proposed the post image processing principle by a direct elimination of the repeated part from each unit-image and arrange them according to the imaging law to provide the complete fingerprint with high resolution. We quantify the repeated imaged areas for the middle microlens and the boundary microlens as follows. For the middle microlens, the middle region of the object sub-fingerprint I with a size of $(2D-D/m)$ is only imaged by the corresponding middle microlens. While for the regions II and II*, they are not only imaged by the middle microlens, but also captured by the upper and lower boundary microlens, respectively. As a result, their images collected by the upper and lower microlens are redundant information and should be omitted from the unit-images. While for the regions III and III*, they are not only imaged by the upper and lower boundary microlenses, respectively, but also captured by the middle microlens, however, their images were omitted from the middle unit-image and are preserved in the unit-images by the upper and lower microlenses, instead. To conclude, for the middle microlens, its effective fingerprint size is D which corresponds to an effective unit-image size of mD with the redundant information size of $(1-m)D$ being omitted. The situation would be a little bit

Optics EXPRESS

different for the boundary microlenes. As for the upper boundary microlens in Fig. 5(a), it images the region III whose information is preserved in the effective unit-image by the middle microlens, thus this part of the unit-image should be omitted. However, for the upper symmetrical region IV, it is only captured by the upper boundary microlens due to the lack of microlens in the upward boundary, thus the effective imaged fingerprint region by the boundary microlens is slightly larger, being $\frac{D}{2}\left(1+\frac{1}{m}\right)$. As for the symmetrical lower microlens, the size of the effective images fingerprint region is same, albeit with a lower additional fingerprint region. Theoretically, when the magnification rate equals 1, the object size equals the image size, meaning no redundant information in each unit-image. With this consideration, it is expected that the whole effective fingerprint image could be reconstructed by using all unit-images, however, it is impractical for operation as the rounded shaped microlenses could not fill the total space completely. We further deduced that the magnification ratio should be equal or less than 0.707 for practical operation in order not to lose effective information of the fingerprint, yielding a minimum device length of $4.12f$.

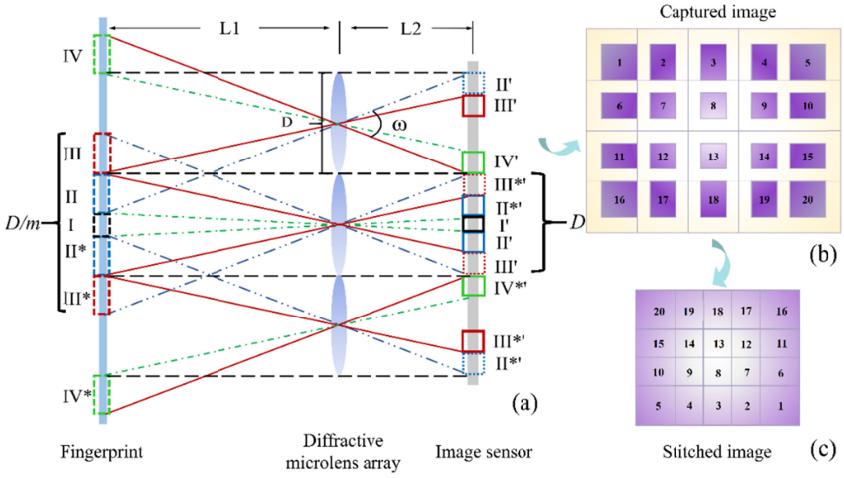

Fig. 5. Principles of the compound image capturing and the reconstruction of the fingerprint information. (a) Schematic illustration for the imaging process of the unit-image by the unit-microlens showing the repeated imaged regions determined by the field of view angle. (b) Schematic illustration for the extraction of the effective information in unit images captured by different microlenses. (c) Reconstruction of the complete fingerprint image by the realignment of extracted effective information in unit-images according to the inverse imaging principle.

Until now, we have only considered a linear distribution of the diffractive microlenses. As for the practical situation, the diffractive microlens array sheet is two-dimensional, which means we have to extend the above 1D imaging cutting and reconstruction method to the 2D case. The reconstruction method for the 2D distribution of microlenses could be simply treated by a combination of the two linear distribution of microlenses in the vertical and parallel directions, however, the microlenses would be classified into three categories instead, which are the center microlens (surrounded by other microlenses in the vertical and parallel directions. For example, the region marked 7 in Fig. 5(b)), the edge microlenses (there is no microlens at one of its edges. For example, the region marked 2 in Fig. 5(b)) and the corner microlenses (there are no microlenses at two of its edges. For example, the region marked 5 in Fig. 5(b)). For the center microlens, the extracted effective image size in the vertical and parallel direction is both mD. For the edge microlens such as the region 2 in Fig. 5(b), its effective size for the unit-image in the parallel and vertical directions is mD and $\frac{D}{2}(1+m)$,

Optics EXPRESS

respectively. As for the corner microlens, the extracted effective image size in the vertical and parallel direction is both $\frac{D}{2}(1+m)$. With this information extraction method, the unit-images by all unit microlenses can be processed to yield the effective information size. The microlens array with 5 × 4 microlenses is shown in Fig. 5(b), and the effective sub-image size for each unit-image is extracted and denoted in purple regions marked with corresponding numbers. As the final step for the reconstruction of the fingerprint image, the extracted regions are re-arranged according to the inverted imaging law as shown in Fig. 5(c), providing a complete fingerprint image without redundant information.

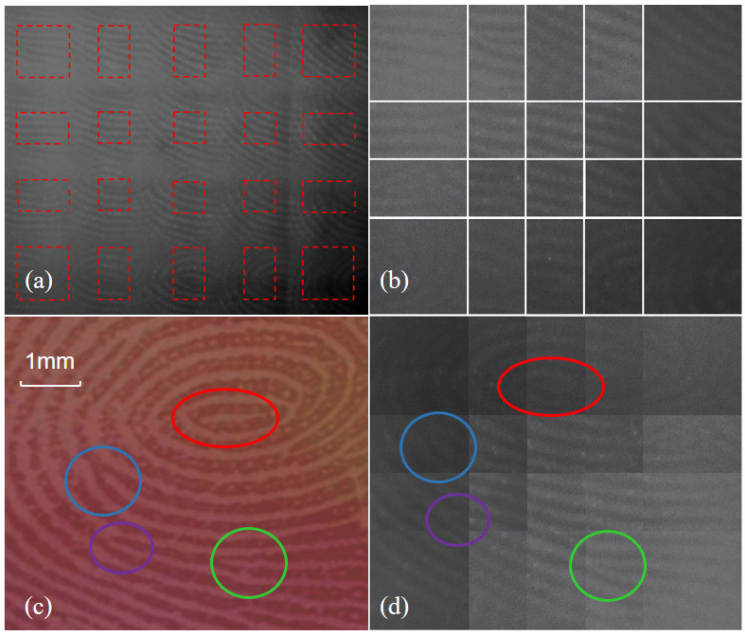

Fig. 6. (a) The compound image constituted by 20 unit-images from the diffractive microlens array. (b) Extracted effective image area from each unit-image. (c) Image of the fingerprint by a camera. (d) Reconstructed fingerprint image from the extracted effective image areas. A comparison between the true fingerprint and the captured fingerprint regarding the details was made by colored regions.

6. Fingerprint capturing and image reconstruction

The compound image captured by the 5 × 4 diffractive microlens array sheet is shown in Fig. 6(a) where the object distance was 4.7 mm and the image distance was 1.2 mm. The compound image consists of 20 unit-images containing information from different regions of the human fingerprint, however, information crosstalk among different unit-images is obvious due to the absence of the opaque wall. Subsequently, the effective imaging region in each unit-image is extracted according to the criterion in Sec. 5 and the extracted effective sub-images depending on the microlens diameter and the magnification ratio are shown in Fig. 6(b). As discussed in Sec. 5, the effective image area from the inner microlens is the smallest, and that from the boundary microlens comes next, while the extracted imaging area from the corner microlens is the largest. The extracted effective subimage regions are realigned according to the inverted imaging law and they are stitched together to yield the complete fingerprint image as shown in Fig. 6(c). The reconstructed fingerprint image contains 856 × 1043 pixels, corresponding to an object area around 6 × 7 mm^2 which is slightly larger than the area of the microlens array. For comparison, the image of the human finger captured by a camera was shown in Fig. 6(d). The reconstructed fingerprint image by the compact

Optics EXPRESS

compound-eye imaging module preserves most details of the fingerprint, albeit with some distortions caused by the misalignment of the optical setup.

7. Conclusion

In conclusion, we have proposed a compact compound-eye imaging module based on the diffractive microlens array and utilize it for biometric fingerprint capturing. As a flat optics, the diffractive microlens array endows the novel imaging system with ultra-thin component thickness, high imaging performance and low cost. The top glass plate not only serves as the backlighting waveguide for illumination but also as the touch panel for fingerprint collection, reducing the total module thickness while exhibiting high compatibility with the display screen. In addition, we have developed a laser direct write system with high resolution gray scale lithography capability to fabricate the diffractive microlens array with a continuous trough morphology, featuring high imaging efficiency when compared with the common amplitude Fresnel lens. An imaging reconstruction method was proposed by extracting the effective imaging area from each unit-image and stitched together to yield the complete fingerprint image according to the imaging law. A microlens array sheet with 5 × 4 diffractive microlenses was fabricated and shows the practicability in the compound-eye imaging module for real fingerprint capturing at a short distance. These results pave a way for the compact module aiming for integrated optical microsystems using the diffractive optics, which are potentially light-weight and low-cost.

Funding

National Natural Science Foundation of China (NSFC) (61505131); Natural Science Foundation of Jiangsu Province (BK20150309, BK20181166); China Postdoctoral Science Foundation (2017T100403); Natural Science Research of Jiangsu Higher Education Institutions of China (18KJB510040, Priority Academic Program Development [PAPD]).

Acknowledgments

We thank support from the Priority Academic Program Development (PAPD) of Jiangsu Higher Education Institutions.

References

1. A. R. Parker and H. E. Townley, "Biomimetics of photonic nanostructures," Nat. Nanotechnol. **2**(6), 347–353 (2007).
2. X. Gao, X. Yan, X. Yao, L. Xu, K. Zhang, J. Zhang, B. Yang, and L. Jiang, "The dry-style antifogging properties of mosquito compound eyes and artificial analogues prepared by soft lithography," Adv. Mater. **19**(17), 2213–2217 (2007).
3. Y. Li, J. Zhang, S. Zhu, H. Dong, F. Jia, Z. Wang, Z. Sun, L. Zhang, Y. Li, H. Li, W. Xu, and B. Yang, "Biomimetic surfaces for high□performance optics," Adv. Mater. **21**, 4731–4734 (2009).
4. K.-H. Jeong, J. Kim, and L. P. Lee, "Biologically inspired artificial compound eyes," Science **312**(5773), 557–561 (2006).
5. D. Floreano, R. Pericet-Camara, S. Viollet, F. Ruffier, A. Brückner, R. Leitel, W. Buss, M. Menouni, F. Expert, R. Juston, M. K. Dobrzynski, G. L'Eplattenier, F. Recktenwald, H. A. Mallot, and N. Franceschini, "Miniature curved artificial compound eyes," Proc. Natl. Acad. Sci. U.S.A. **110**(23), 9267–9272 (2013).
6. J. Tanida, T. Kumagai, K. Yamada, S. Miyatake, K. Ishida, T. Morimoto, N. Kondou, D. Miyazaki, and Y. Ichioka, "Thin observation module by bound optics (TOMBO): concept and experimental verification," Appl. Opt. **40**(11), 1806–1813 (2001).
7. R. Shogenji, Y. Kitamura, K. Yamada, S. Miyatake, and J. Tanida, "Multispectral imaging using compact compound optics," Opt. Express **12**(8), 1643–1655 (2004).
8. R. Horisaki, Y. Nakao, T. Toyoda, K. Kagawa, Y. Masaki, and J. Tanida, "A thin and compact compound-eye imaging system incorporated with an image restoration considering color shift, brightness variation, and defocus," Opt. Rev. **16**(3), 241–246 (2009).
9. D. Wu, J.-N. Wang, L.-G. Niu, X. L. Zhang, S. Z. Wu, Q.-D. Chen, L. P. Lee, and H. B. Sun, "Bioinspired fabrication of high-quality 3D artificial compound eyes by voxel-modulation femtosecond laser writing for distortion-free wide-field-of-view imaging," Adv. Opt. Mater. **2**(8), 751–758 (2014).
10. R. Shogenji, Y. Kitamura, K. Yamada, S. Miyatake, and J. Tanida, "Bimodal fingerprint capturing system based on compound-eye imaging module," Appl. Opt. **43**(6), 1355–1359 (2004).

Optics EXPRESS

11. H. C. Ko, M. P. Stoykovich, J. Song, V. Malyarchuk, W. M. Choi, C.-J. Yu, J. B. Geddes 3rd, J. Xiao, S. Wang, Y. Huang, and J. A. Rogers, "A hemispherical electronic eye camera based on compressible silicon optoelectronics," Nature **454**(7205), 748–753 (2008).
12. P. Genevet, F. Capasso, F. Aieta, M. Khorasaninejad, and R. Devlin, "Recent advances in planar optics: from plasmonic to dielectric metasurfaces," Optica **4**(1), 139–152 (2017).
13. M. Hain, W. von Spiegel, M. Schmiedchen, T. Tschudi, and B. Javidi, "3D integral imaging using diffractive Fresnel lens arrays," Opt. Express **13**(1), 315–326 (2005).
14. A. Özdemir, N. Yılmaz, S. A. Alboon, Y. Takashima, and H. Kurt, "Analysis of the focusing crosstalk effects of broadband all-dielectric planar metasurface microlens arrays for ultra-compact optical device applications," OSA Continuum **1**(2), 506–520 (2018).
15. N. Davidson and N. Bokor, "High-numerical-aperture focusing of radially polarized doughnut beams with a parabolic mirror and a flat diffractive lens," Opt. Lett. **29**(12), 1318–1320 (2004).
16. A. Ozer, N. Yilmaz, H. Kocer, and H. Kurt, "Polarization-insensitive beam splitters using all-dielectric phase gradient metasurfaces at visible wavelengths," Opt. Lett. **43**(18), 4350–4353 (2018).
17. B. Katz, J. Rosen, R. Kelner, and G. Brooker, "Enhanced resolution and throughput of Fresnel incoherent correlation holography (FINCH) using dual diffractive lenses on a spatial light modulator (SLM)," Opt. Express **20**(8), 9109–9121 (2012).
18. P. J. Sonneveld, G. L. A. M. Swinkels, B. A. J. Tuijl, H. J. J. Janssen, J. Campen, and G. P. A. Bot, "Performance of a concentrated photovoltaic energy system with static linear Fresnel lenses," Sol. Energy **85**(3), 432–442 (2011).
19. Z. Kuang, D. Liu, W. Perrie, S. Edwardson, M. Sharp, E. Fearon, G. Dearden, and K. Watkins, "Fast parallel diffractive multi-beam femtosecond laser surface micro-structuring," Appl. Surf. Sci. **255**(13-14), 6582–6588 (2009).
20. P. Sun, Z. Liu, W. Wang, L. Ma, D. Shen, W. Hu, Y. Lu, L. Chen, and Z. Zheng, "Light-reconfigured waveband-selective diffraction device enabled by micro-patterning of a photoresponsive self-organized helical superstructure," J. Mater. Chem. C Mater. Opt. Electron. Devices **4**(39), 9325–9330 (2016).
21. A. K. Jain, A. Ross, and S. Prabhakar, "An introduction to biometric recognition," IEEE T. Circ. Syst. Vid. **14**(1), 4–20 (2004).
22. J. Yang, J. Chen, Y. Su, Q. Jing, Z. Li, F. Yi, X. Wen, Z. Wang, and Z. L. Wang, "Eardrum-inspired active sensors for self-powered cardiovascular system characterization and throat-attached anti-interference voice recognition," Adv. Mater. **27**(8), 1316–1326 (2015).
23. K. H. Fielding, J. L. Horner, and C. K. Makekau, "Optical fingerprint identification by binary joint transform correlation," Opt. Eng. **30**(12), 1958–1962 (1991).
24. A. Kumar and C. Kwong, "Towards contactless, low-cost and accurate 3D fingerprint identification," in Proceedings of the IEEE Conference on Computer Vision and Pattern Recognition (2013), pp. 3438–3443.
25. R. D. Labati, A. Genovese, V. Piuri, and F. Scotti, "Toward unconstrained fingerprint recognition: a fully touchless 3-D system based on two views on the move," IEEE T. Syst. Man. Cy-S. **46**, 202–218 (2016).
26. Y.-G. Lee, S.-U. Baek, S.-S. Lee, and G.-S. Son, "Miniaturized optical fingerprint scanner incorporating an integrated encoding plate," Microw. Opt. Technol. Lett. **60**(1), 122–126 (2018).
27. B. Morgan, C. M. Waits, J. Krizmanic, and R. Ghodssi, "Development of a deep silicon phase Fresnel lens using gray-scale lithography and deep reactive ion etching," J. Microelectromech. Syst. **13**(1), 113–120 (2004).
28. X.-Q. Wang, W.-Q. Yang, Z. Liu, W. Duan, W. Hu, Z.-G. Zheng, D. Shen, V. G. Chigrinov, and H.-S. Kwok, "Switchable Fresnel lens based on hybrid photo-aligned dual frequency nematic liquid crystal," Opt. Mater. Express **7**(1), 8–15 (2017).
29. M. J. Moghimi, J. Fernandes, A. Kanhere, and H. Jiang, "Micro-fresnel-zone-plate array on flexible substrate for large field-of-view and focus scanning," Sci. Rep. **5**(1), 15861 (2015).